

Electronic supplementary material

Phase behaviour and thermoelastic properties of perdeuterated ammonia hydrate and ice polymorphs from 0—2 GPa.

*A. D. Fortes, I. G. Wood, L. Vočadlo, K. S. Knight, W. G. Marshall, M. G. Tucker,  
& F. Fernandez-Alonso*

This deposit contains additional text describing details of the experimental data collection, additional illustrations reporting our neutron powder diffraction data, and additional tables. Where supplementary figures are referred to, these are numbered in the format, Fig. S1, etc., whereas figures in the main body of the paper are simply, Fig. 1, etc.

## **1. Experimental details.**

At a pulsed spallation neutron source like ISIS it is customary to specify the data collection time in terms of the integrated proton current on the target, since this allows for (often significant) deviations of the beam current from its typical value of 170-180  $\mu\text{A}$ , or periods in which the beam is off altogether, and allows for comparison between instruments which receive neutron pulses at different rates (e.g., HRPD vs. PEARL/HiPr). For clarity, we specify both the integrated proton current in  $\mu\text{A hr}$ , and the actual amount of time spent collecting a given dataset.

## Electronic supplementary material

### **Experiment 1 (P,T path shown in Figure S1a)**

**Experiment reference number: RB 13234**

**Date of experiment: 6<sup>th</sup> - 8<sup>th</sup> February 2003**

**Instrument: HRPD**

**Sample environment: Al 7075 alloy gas pressure vessel (He gas)**

The objective of this experiment was to measure the thermal expansion and incompressibility of the cubic low-pressure phase of ammonia dihydrate (ADH I), and to search for any evidence of polymorphism either at low temperatures, or at pressures up to 460 MPa.

The sample was introduced to the neutron beamline at a temperature of 174 K under a nominal pressure of 41 MPa, having undergone a prior series of thermal cycles to crystallise ADH I. The specimen was found (by Rietveld refinement) to consist of a mixture of ADH I and ~ 12.5 wt. % ice Ih. The pressure was stepped up (using helium as the pressure transmitting medium) in intervals of ~50 MPa, counting for ~ 15 minutes per datum, to the maximum rated pressure of the aluminium cell (~460 MPa). At 350 MPa (point A in [Fig. S1a](#)) there was a drop in pressure, and the Bragg peaks of ice Ih were replaced by reflections due to a tetragonal ice polymorph having a  $c/a$  ratio commensurate with being ice IX (Londono *et al.*, 1993). The occurrence of metastable IX rather than ice II, which is the stable phase under these P,T conditions, may be due to some effect of preferential nucleation on an ADH substrate, the effect of sluggish kinetics, or due to the compression rate (*cf.*, Bauer *et al.*, 2008). Ice IX persisted as an accessory phase up to the maximum pressure investigated. The anticipated phase transition to ADH II had not occurred at 460 MPa, so the sample was warmed by 5 K whereupon partial melting occurred to a slurry of ice IX crystals in ammonia-water liquid (B). When cooled back to 174 K at 443 MPa (C), new Bragg peaks appeared over a period of several hours ([Figure S2](#)). Diffraction data were then collected at 174 K for ~ 11 hours (337  $\mu\text{A hr}$ ) in the 30—130 ms t-o-f window, and for ~90 minutes (51  $\mu\text{A hr}$ ) in the 100—200 ms window. The sample was then cooled in 5 K steps to 140 K (counting for 20 minutes - 10  $\mu\text{A hr}$  - with 10 minutes of thermal equilibration at each point), quenched to 112 K (D) and subsequently decompressed to ~50 MPa (E); peaks from the high-pressure phase mixture persisted, albeit with a considerable degree of strain broadening when the pressure was completely released.

## Electronic supplementary material

### **Experiment 2 (P,T path shown in Figure S1b)**

**Experiment reference number: RB14485**

**Date of experiment: 1<sup>st</sup> - 5<sup>th</sup> March 2004**

**Instrument: HRPD**

**Sample environment: TiZr alloy gas pressure vessel (He gas)**

This experiment extended the pressure range of the earlier study to the maximum pressure achievable using the ISIS gas cells, 550 MPa, with the objective of identifying the solid-solid phase transition anticipated from the dilatometry measurements (Hogenboom *et al.*, 1997), but not observed in experiment 1.

Aqueous solution was pipetted into a TiZr gas pressure vessel and sealed under 10 MPa of He gas. After offline temperature cycling to form ADH I, the pressure was increased directly to 550 MPa at 174 K. This resulted in a change in the diffraction pattern, and data were collected at this P,T point (**A**) in the 30—130 ms t-o-f window for ~ 13½ hours (446  $\mu$ A hr). Subsequently, the choppers were re-phased and data were collected in the 100—200 ms t-o-f window for ~ 21 hours (703  $\mu$ A hr); these combined diffraction patterns are shown in **Fig. S8a**. The specimen was then warmed in 2 K increments from 174 K to 190 K, collecting data in the 30-130 ms window for 30 minutes (17  $\mu$ A hr) per datum (except for 178 K, where data were integrated for 37  $\mu$ A hr). At 190 K (**B**), a change in the diffraction pattern indicative of a phase transition was observed and so a further long integration was done. Data were collected at 550 MPa, 190 K for ~16 hours (521  $\mu$ A hr) in the 30—130 ms t-o-f window and for a further 16 hours (512  $\mu$ A hr) in the 100—200 ms window; these combined patterns are shown in **Fig. S9b**. Finally, the sample was cooled in 5 K increments from 190 K to 155 K with data being collected for ~ 1 hour (30  $\mu$ A hr) at each point.

Electronic supplementary material

**Experiment 3** (P,T path shown in Figure S1c)

**Experiment reference number: RB20049 (first attempt)**

**Date of experiment: December 6<sup>th</sup> - 8<sup>th</sup> 2004**

**Instrument: OSIRIS**

**Sample environment: TiZr alloy gas pressure vessel (He gas)**

The objective of this experiment was to reproduce the phase transitions observed in experiment 2, and make measurements at long d-spacings in order to facilitate indexing of the powder patterns.

Aqueous ammonia solution was loaded into a TiZr pressure vessel as in experiment 2, and sealed under 15 MPa of helium gas. Offline temperature cycling failed to cause crystallisation of the specimen, most likely due to a programming error than to any failure of the sample to respond. As a result, temperature cycling from 173—179 K was carried out in the beam-line (**A**); the details of this process are given in section 3.2. Once crystallisation of ADH I was complete, after approximately 14 hours, the pressure was increased directly to 550 MPa at 175 K (**B**). We observed that the Bragg peaks of ADH I had been replaced by a new set of peaks (**Fig. S8b**) which shared some similarities with those of ADH II as measured by Nelmes *et al.* (1999). At this point it was discovered that there was a small though manageable leak in the high-pressure cell, venting He gas into the tail of cryostat. Diffraction data were collected sequentially at 550 MPa, 175 K in d-ranges 1 through 8 (0.7—10.0 Å), measuring for 10 μA hr in d-range 1, 20 μA hr in d-range 2, and so on up to 80 μA hr in d-range 8 (total 360 μA hr, or ~ 2 hours). This cycle of data collection was repeated a further two times, after which a mechanical failure at ISIS synchrotron ended the experiment.

**Experiment 4** (P,T path shown in Figure S1d)

**Experiment reference number: RB20049 (second attempt)**

**Date of experiment: 17<sup>th</sup> - 21<sup>st</sup> February 2005**

**Instrument: OSIRIS**

**Sample environment: TiZr alloy gas pressure vessel (He gas)**

This experiment was a direct continuation of experiment 3, which had been prematurely cut short.

## Electronic supplementary material

As in experiment 3, aqueous solution was loaded into a TiZr cell with silica wool and sealed under 15 MPa of He gas. Offline temperature cycling failed to induce crystallisation, and so this was done in the beam-line, as described further in section 3.2. At the end of ~18 hours of temperature cycling from 173—178 K (**A**), the temperature was stabilised at 173 K, and the pressure was increased directly to 425 MPa (**B**). Inspection of diffraction data collected in d-range 2 at both 425 and 450 MPa (21  $\mu$ A hr each) revealed the Bragg peaks of ADH I with accessory ice IX and very small peaks due to AMH I. Data collected at 475 MPa exhibited evidence of very weak new Bragg reflections, and a slight decrease in the intensity of ADH I peaks. Subsequent measurements at 500, 525, and 550 MPa (also 21  $\mu$ A hr each), yielded a diffraction pattern in very close agreement with that reported for ADH II by Nelmes *et al.* (1999). As shown in **Figure S3**, following the Bragg peaks through the transition allows clear identification of ice IX, AMH I, and of some residual ADH I, in the diffraction pattern, which made it possible to isolate the unique ADH II peaks for indexing purposes. Data were collected sequentially at 546 MPa, 173 K (**C**) in d-ranges 2 through 4 (1.8—6.0 Å), counting for 60, 90, and 120  $\mu$ A hr, respectively, this cycle of observations being repeated six times (total 1620  $\mu$ A hr or ~ 9 hours); the high resolution component of this data set is shown in **Fig. S8c**.

The sample was warmed in 5 K increments to 188 K, with short counts (12  $\mu$ Ahr) being made at each point. At 188 K (**D**), new Bragg peaks were observed alongside those of ADH II, and after increasing the temperature to 190 K, ADH II had been completely eliminated (**Figure S4**). Data were collected at 546 MPa, 190 K in d-ranges 2 through 4 for a total of 934  $\mu$ A hr (~ 5¼ hours); the high resolution component of this data set is shown in **Fig. S9c**. Further warming in 2 K increments (13-14  $\mu$ A hr per point) resulted in the onset of melting at 196 K (**E**); we held this temperature to observe the progress of melting over a series of integrations, at the end of which we believed the specimen to be completely molten. However, in **Figure S5** it is clear that after proper correction for the sample environment, Bragg peaks from ice II are still present, and indeed persist up to 210 K. Subsequent attempts to refreeze the liquid at 550 MPa failed.

## Electronic supplementary material

### **Experiment 5 (P,T path shown in Figures S1e, S1f, and S1g)**

**Experiment reference number: RB 13233**

**Date of experiment: 7<sup>th</sup> - 10<sup>th</sup> July 2003**

**Instrument: PEARL/HiPr**

**Sample environment: Paris-Edinburgh cell, TiZr encapsulated gaskets**

The objective of this study was to make an initial survey of any polymorphism in ammonia dihydrate up to ~ 10 GPa.

A total of three separate loadings of the P-E cell were studied during this experiment, with samples of aqueous ammonia soaked into a wad of silica wool and loaded with a chip of Pb foil. Loads of 12—13 tons were applied at room temperature, followed by cooling to 170 K. During this process, diffraction patterns were integrated over ~30 minute periods so as to observe the process of crystallisation.

Loading one (**Figure S1e**). Following crystallisation of the sample under a load of 14.8 tons at 175 K (**A**), diffraction data were integrated for ~ 5 hours (900  $\mu\text{A hr}$ ). We ascertained subsequently that the material produced under these conditions was a mixture of AMH II and a high-pressure polymorph of ammonia dihydrate which we called ADH IV. This mixture was subsequently examined under loads of 24.8 and 29.8 tons: at the latter datum, after approximately 15 minutes, the load dropped suddenly to 20 tons (**B**) and the diffraction pattern indicated that amorphisation of the specimen had taken place. Further increases in load caused three very broad 'peaks' to emerge (indicative of a poorly diffracting nanocrystalline material) on top of a residual amorphous feature. At a load of 63 tons (**C**), a single body-centred cubic phase formed, and pertinent details of this are reported in Fortes *et al.* (2007); this bcc-phase has since been reproduced by Loveday *et al.* (2009). The bcc-phase persisted on unloading directly from 80 to 15 tons at 190 K (**D**); subsequent reduction of the load to 1.8 tons resulted in crystallisation of the phase which we subsequently identified as ADH IV (**Figure S6d**); data were collected at 1.8 tons, 190 K for 30 minutes.

Loading two (**Figure S1f**). This sample proved to be significantly off stoichiometry due to a chemical reaction between the specimen and the bush of the syringe needle which formed a sky-blue copper-ammonia aqueous liquid. Initial cooling (**A**) resulted in the formation of ice VI + amorphous material at 15.3 tons, 170 K (**Figure S6a**), and data were collected at this point for 13 hours (2340  $\mu\text{A hr}$ ), ostensibly in the hope that another phase would crystallise. However, warming to 183 K (15.6 tons) caused the residual amorphous

## Electronic supplementary material

material to crystallise (suggesting that it was either a supercooled liquid or a glassy solid), and once the temperature had stabilised near 190 K (**B**) we made a 7 hour integration (1260  $\mu\text{A hr}$ ), shown in **Figure S6b**. Data were then collected under loads of 20.7 and 25.8 tons; beyond these loads, the patterns grew to resemble those seen post amorphisation in loading one, and despite the transformation of ice VI to ice VIII at 30.5 tons (**C**) there is little else of interest to note.

Loading three (**Figure S1g**). Initially, this loading produced what appeared to be a mixture of ice VI, ADH IV, and amorphous material under a load of 9.8 tons at 170 K (**A**). This was melted by warming to 195 K: increasing the load on the liquid from 10.6 to 16.3 tons resulted in pressure-freezing to the phase identified as ADH IV (**B**). We made a 5 hour integration (900  $\mu\text{A hr}$ ) at 16.6 tons, 195 K, depicted in **Figure S6c**. Shorter counts were collected at 21.9, 26.7, and 39.2 tons, the diffraction peaks becoming increasingly strain broadened and difficult to identify with increasing pressure. The specimen finally disproportionated to a mixture of AMH VI and ice VIII under a load of 77.9 tons (**C**) (see Fortes *et al.*, 2007).

### **Experiment 6 (P,T path shown in Figure S1h)**

**Experiment reference number: RB 15134**

**Date of experiment: 12<sup>th</sup> - 16<sup>th</sup> November 2004**

**Instrument: PEARL/HiPr**

**Sample environment: Paris-Edinburgh cell, TiZr encapsulated gaskets**

The purpose of this experiment was to follow up the initial survey (experiment 5) with a series of longer integrations of ADH IV without the use of a Pb pressure calibrant.

The sample loading procedure was the same, but the time required for crystallisation to occur (~ 24 hours) was much greater, eventually occurring under a load of 16.8 tons at 170 K (**A**). Two long integrations were made at 190 K, the first under loads between 15.5 - 16.7 tons (12 hr, 2160  $\mu\text{A hr}$ ) from a mixture of ADH IV and ice II (shown in **Fig. S11**), and the second under loads between 24.3 and 25.8 tons (12.5 hr, 2225  $\mu\text{A hr}$ ) where co-existing ice II had transformed to ice VI (**B**). Shorter counts were made at 29.0, 34.5, 39.5, and 44.8 tons at 190 K. Warming the specimen to 225 K at 44.8 tons resulted in disproportionation to AMH VI + ice VIII (**C**).

Electronic supplementary material

**Experiment 7** (P,T path shown in Figure S1i)

**Experiment reference number: RB 520044 (first attempt)**

**Date of experiment: 16<sup>th</sup> - 17<sup>th</sup> November 2005**

**Instrument: PEARL/HiPr**

**Sample environment: Paris-Edinburgh cell, TiZr encapsulated gaskets**

The objective of this experiment was to investigate the behaviour of ADH IV upon warming, to determine either the melting point, or the point at which disproportionation to AMH + ice occurs as a function of pressure.

Stoichiometric liquid was loaded with silica wool and lead powder. Crystallisation of an ice VI + ADH mixture took place at 22 tons, 190 K (A). Diffraction patterns were collected on warming under a load of 25 tons in 10 K increments from 190 - 220 K, and 5 K increments thereafter, counting for one hour with 30 minutes of warming and equilibration at each datum. At 240 K (B), the sample was observed to have undergone partial melting to ice VI + liquid (Figure S7). During a four hour period in which the proton beam was off, the sample was unloaded to 15 tons and cooled to 190 K (C), causing re-crystallisation of ADH IV + ice VI. The load and temperature were increased directly to 25 tons, 220 K, and data were integrated for four hours (720  $\mu$ A hr). After increasing the load to 32.5 tons and warming to 235 K (D), the experiment was ended by a failure of the ISIS synchrotron.

**Experiment 8** (P,T path shown in Supplementary Figure S1j)

**Experiment reference number: RB 520044 (second attempt)**

**Date of experiment: 9<sup>th</sup> - 12<sup>th</sup> February 2006**

**Instrument: PEARL/HiPr**

**Sample environment: Paris-Edinburgh cell, TiZr encapsulated gaskets**

In this experiment, the lead powder used in experiment 7 was eschewed in favour of foil, on the grounds that it was not possible to mix sufficient powder with the specimen for the Pb Bragg peaks to be strong enough. In the first loading, ice VI crystallised at 15 tons, 200 K, and further attempts to crystallise ADH IV over a period of ~ 6 hours, involving raising the load up to 25.5 tons, failed and the loading was aborted.

In the second loading of this experiment (Figure S1j), the specimen was held at 15 tons, 190 K for 24 hours offline. Upon mounting in the neutron beam-line, we found that the

## Electronic supplementary material

specimen was single phase ADH IV, and data were collected at 15 tons, 190 K (**A**) for 3.1 hours (560  $\mu\text{A hr}$ ). When the load and temperature were raised to 25 tons, 230 K (**B**), peaks due to ice VI appeared along with those of ADH IV; these can only be due to crystallisation of some residual amorphous material. Data were collected at this P,T point for 5 hours (900  $\mu\text{A hr}$ ). Shorter counts (15 min, 45  $\mu\text{A hr}$ ) at 230 K were made on loading to 28, 31, and 34 tons, where the specimen undergoes a phase transition, the nature of which we have not yet determined (**C**).

**Figure S1**

Panels (a)—(j) report the pressure-temperature paths followed during the eight experiments which contributed data to this paper. In each panel, open circles record P,T points at which diffraction data were integrated whilst the solid black lines and arrows depict the path followed between points. Bold letters highlight specific events referred to in the text that deals with each panel. Shaded boxes show the data points which are reproduced in [Figures S2—S11](#) (continued on the following page).

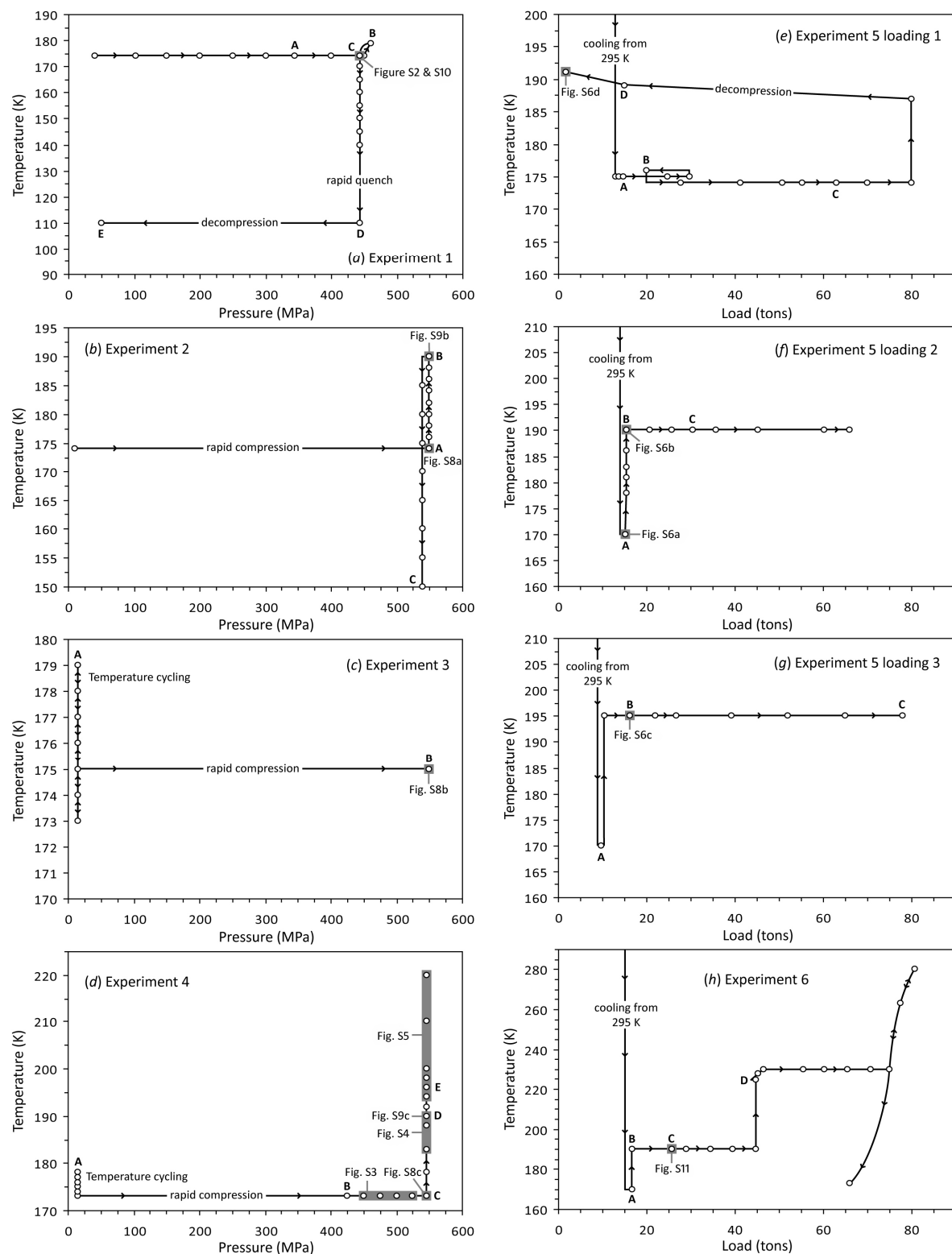
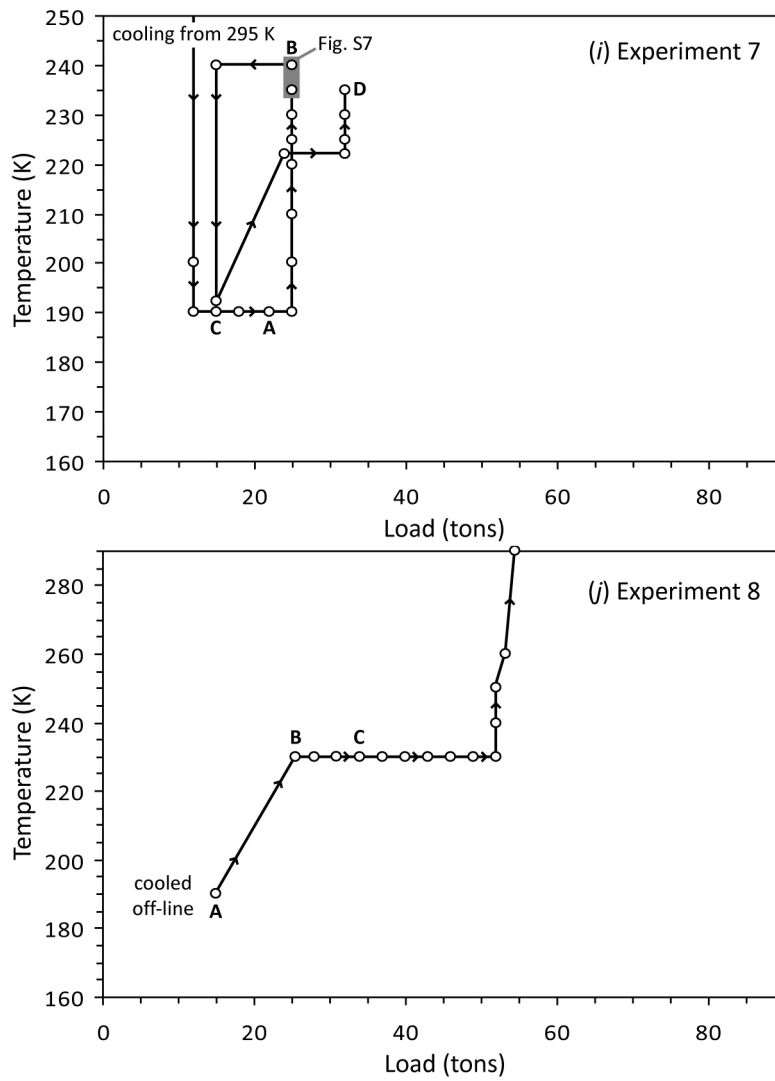


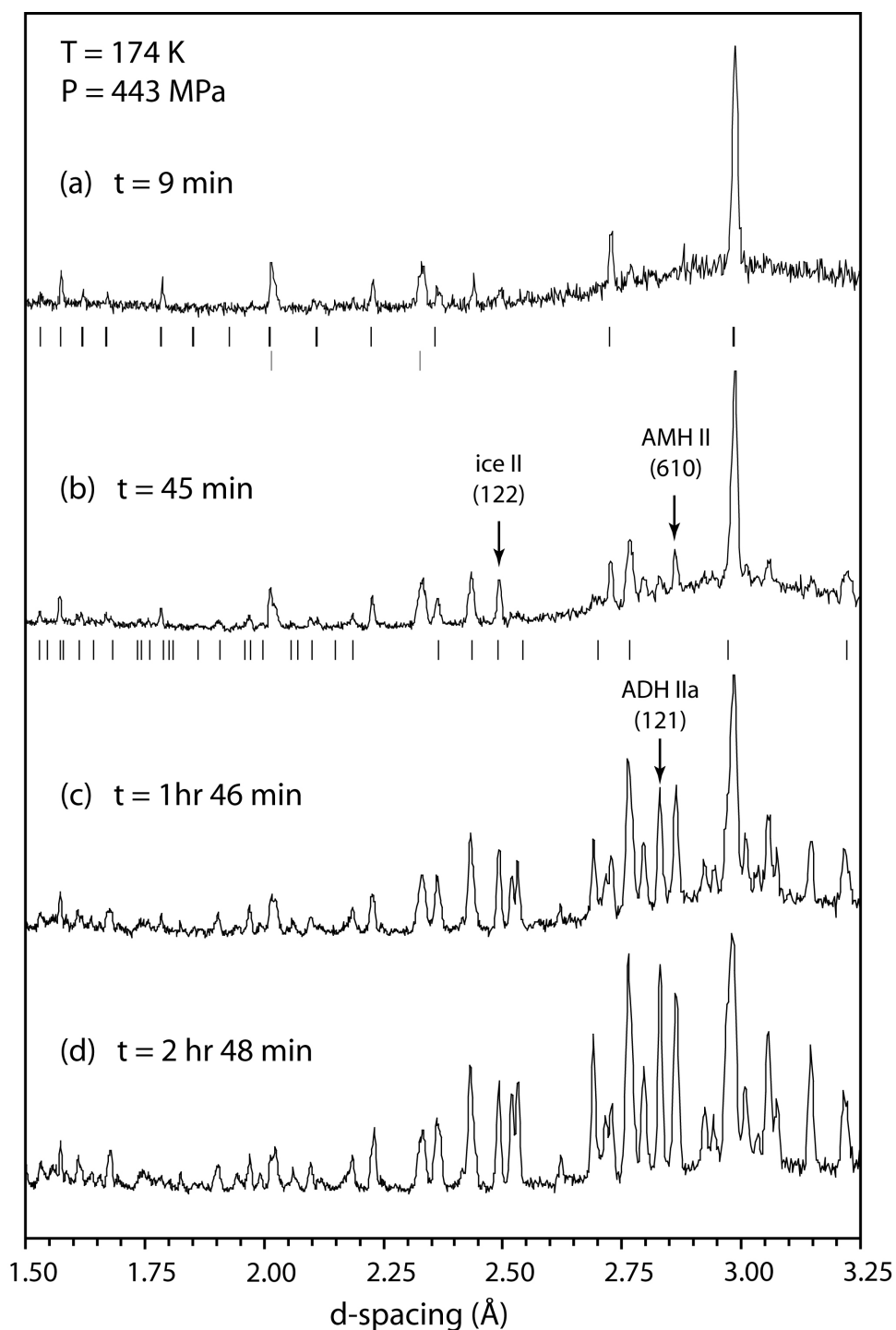
Figure S1, continued from previous page



## Electronic supplementary material

### Figure S2: (Experiment 1)

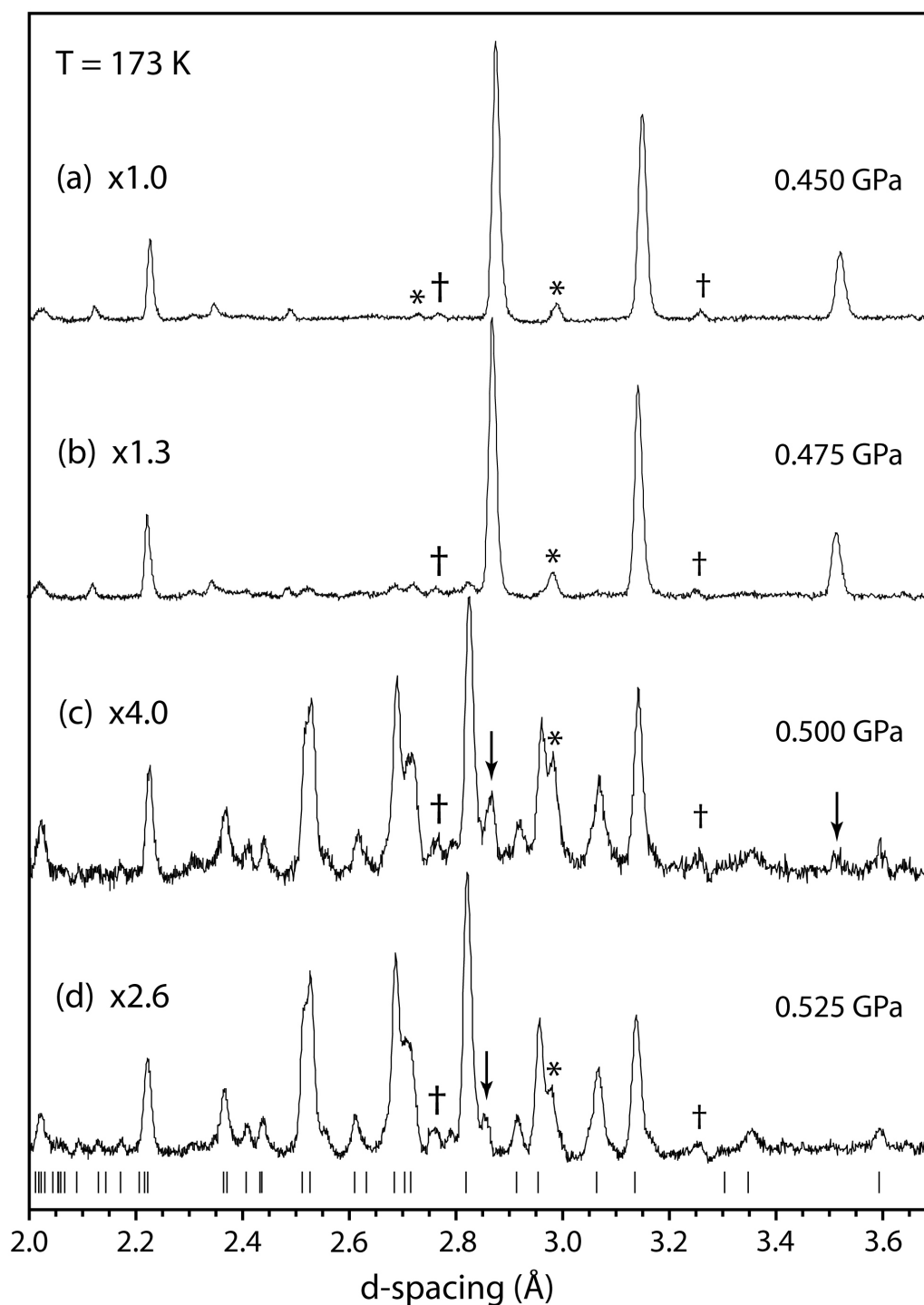
Diffraction patterns acquired at 443 MPa after warming a mixture of ADH I + ice IX from 174 K to 179 K, partial melting, and subsequent cooling back to 174 K; individual captions indicate the time elapsed from cooling back to 174 K. Pattern (a) is of ice IX (upper set of tick marks) in liquid - which is responsible for the broad amorphous feature centred near 3.0 Å - and aluminium (lower tick marks) from the pressure vessel. Pattern (b) is annotated with tick marks for ice II; the three arrowed reflections are those used in the kinetic analysis in section 4.2., and their growth may be followed in patterns (c) and (d). All of these patterns are shown with the same vertical scale factor (contrast [Figures S3 and S4](#)).



## Electronic supplementary material

### Figure S3: (Experiment 4)

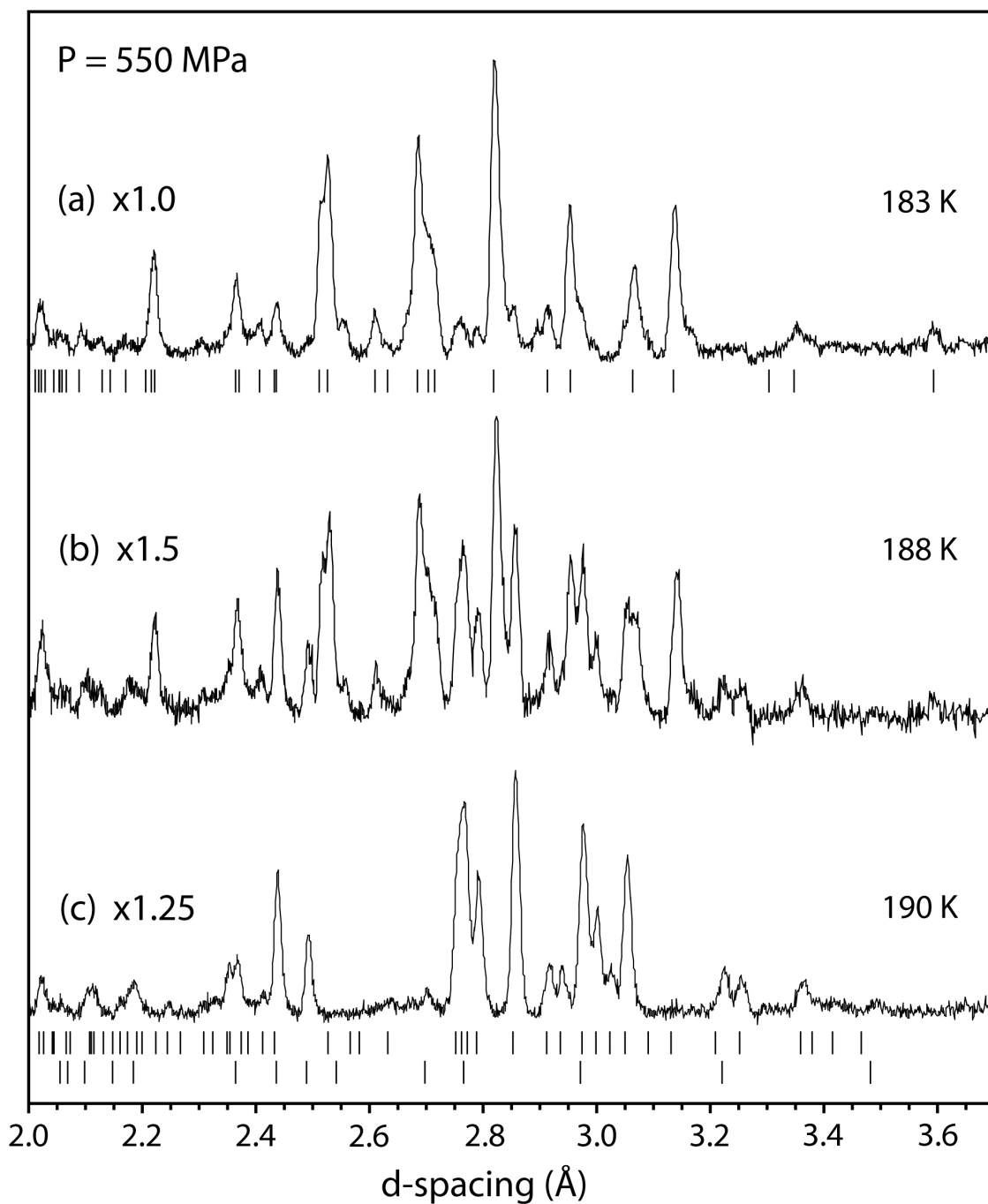
Diffraction patterns acquired at 173 K upon loading a specimen of ADH I + ice IX + ammonia monohydrate I through the ADH I  $\rightarrow$  II transition, with pressure increasing from (a) to (d). Intensities have been multiplied by a scaling factor to reflect the fact that in ADH II the lower symmetry distributes intensity into more reflections, and so these are weaker. Even at 475 MPa, the onset of the transition is marked by a drop in the intensity of the ADH I peaks. Accessory ice IX (asterisks), and AMH (crosses) persist through the transition, as does a small quantity of residual ADH I (arrows). Beneath pattern (a) are the tick marks for ADH I, and beneath pattern (d) are the tick marks for ADH IIa.



## Electronic supplementary material

### Figure S4: (Experiment 4)

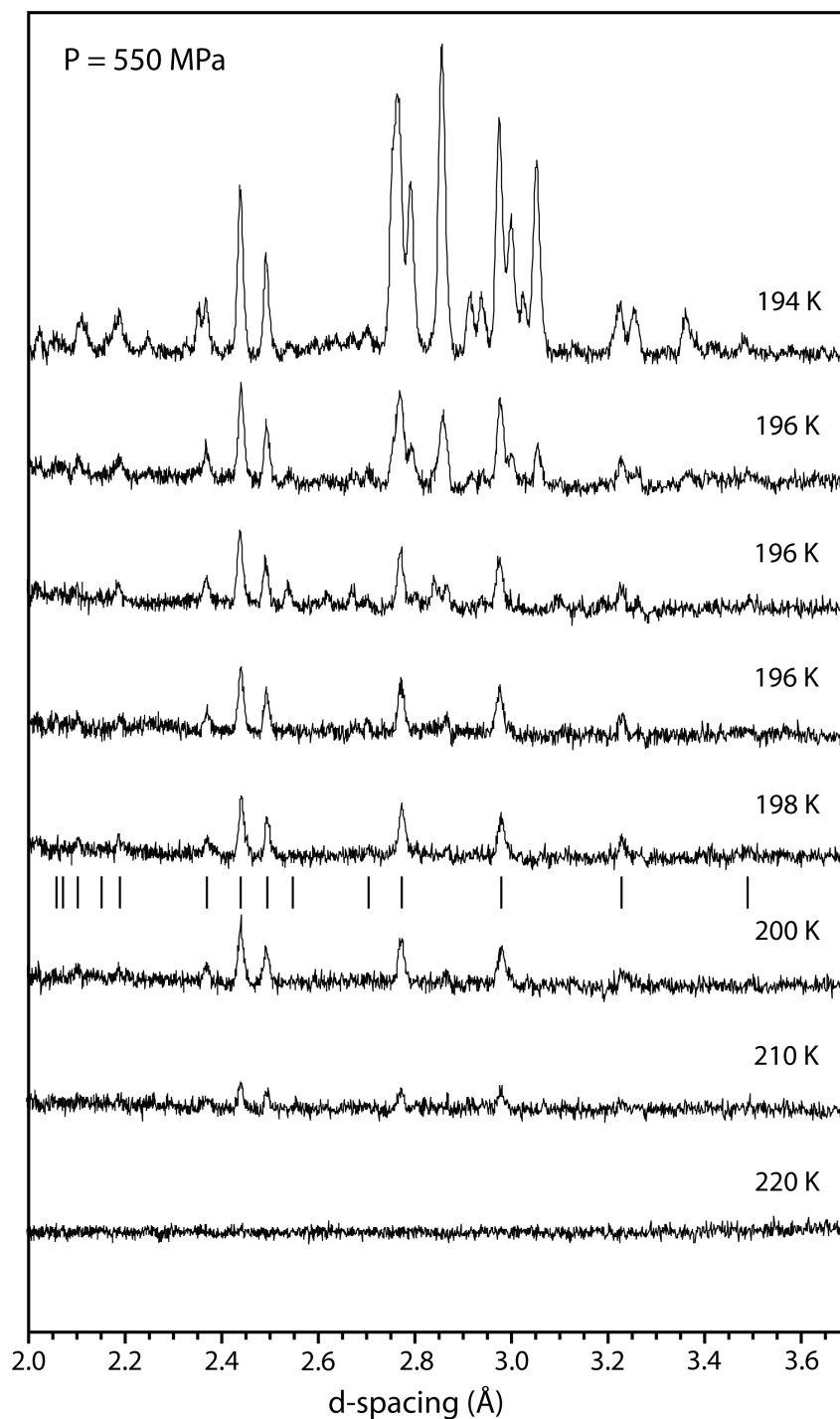
Diffraction patterns acquired upon warming ADH IIa at 550 MPa. As in [Figure S3](#), intensities have been scaled to reflect changes in the distribution of scattering during the transition from ADH II to AMH II + ice II. Tick marks beneath (a) are those for ADH IIa, and those under pattern (c) are for AMH II (upper set) and ice II (lower set).



## Electronic supplementary material

### Figure S5: (Experiment 4)

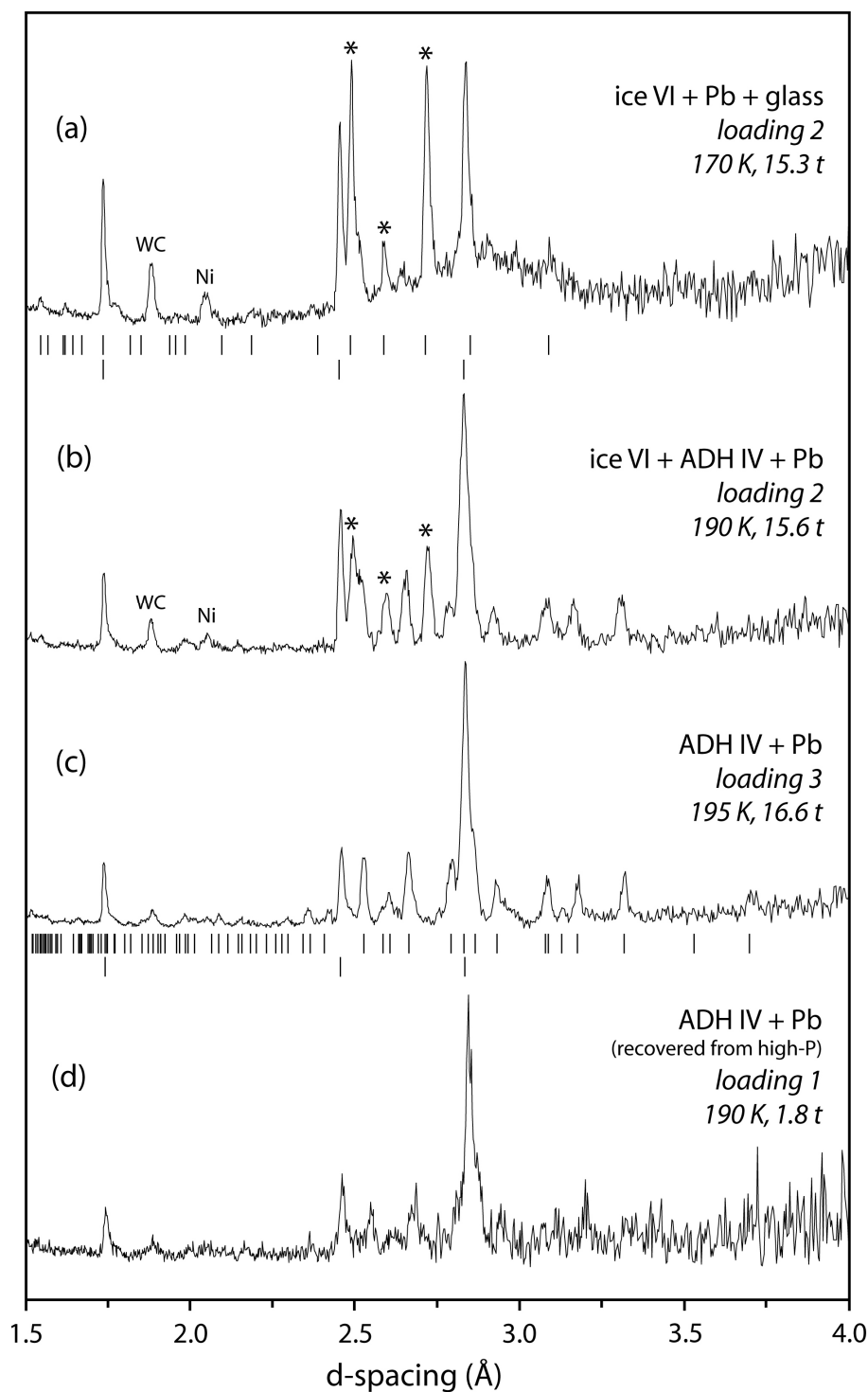
Diffraction patterns acquired upon warming a mixture of AMH II + ice II at 550 MPa, showing the partial melting of the mixture to ice II + liquid at 196 K. Peaks due to ice II (tick marks beneath the 198 K pattern), which persist up to 210 K, had not been seen previously in data uncorrected for sample environment contributions; those between 2.4—2.6 Å were masked by a cluster of peaks from the cryostat tails, and the other weak residual peaks had been attributed wrongly to metallic components in the Bridgman seal of the pressure vessel.



## Electronic supplementary material

### Figure S6: (Experiment 5)

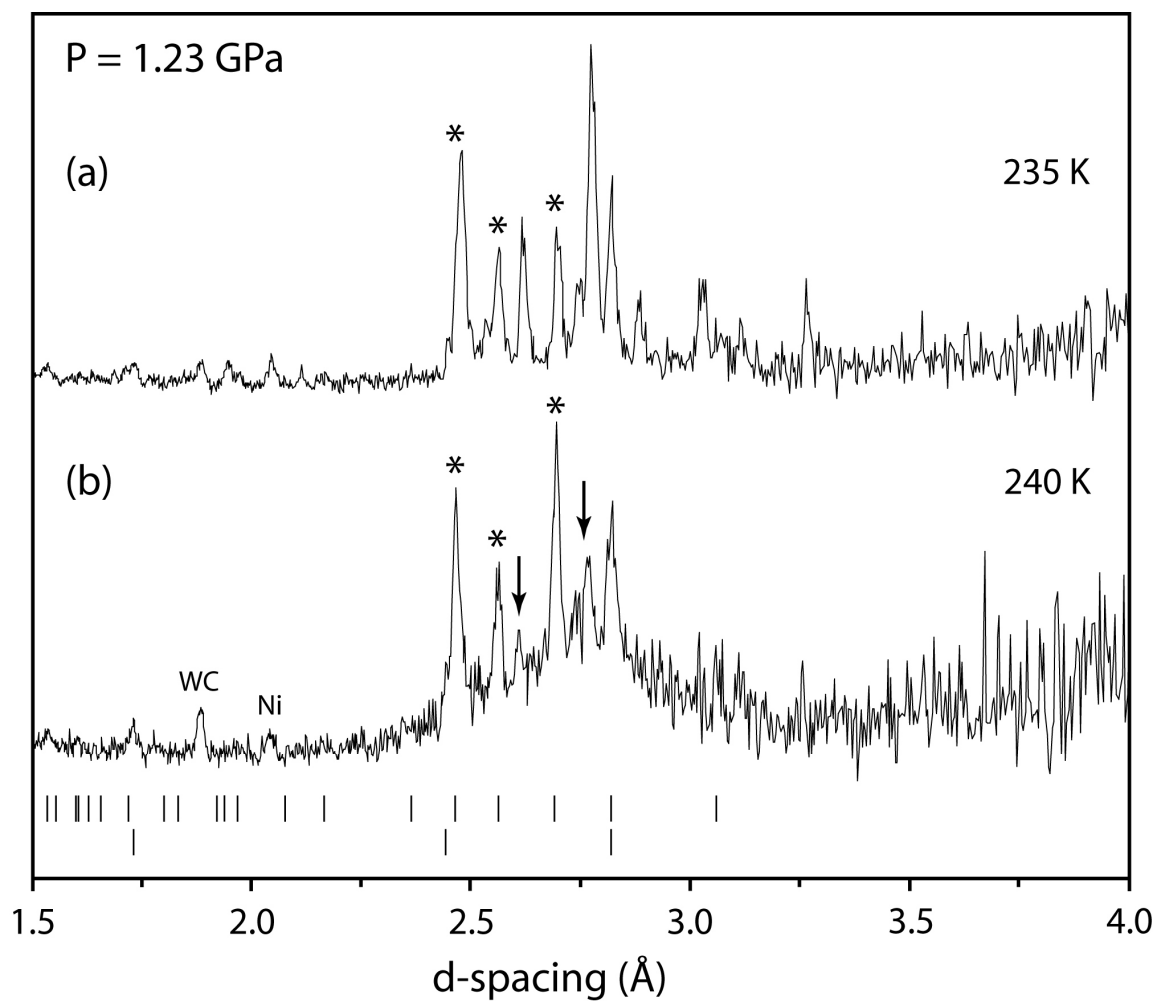
In (a) and (b) we observed first the crystallisation of ice VI (co-existing with some amorphous material) and subsequent growth of ADH IV upon warming. Tick marks beneath (a) are for ice VI (upper set) and the lead pressure calibrant (lower set); the three strongest ice VI reflections are highlighted with asterisks. Scattering from tungsten carbide and nickel binder in the P-E cell's anvils are marked (WC and Ni). In pattern (c) we observed ADH IV without ice VI, and the tick marks are for that phase alone. ADH IV was also observed after decompression of a high-pressure body centred cubic phase (pattern d).



## Electronic supplementary material

### Figure S7: (Experiment 7)

Diffraction data collected during the partial melting of an ADH IV + ice VI mixture at  $\sim 1.23$  GPa; tick marks under pattern (b) are for ice VI (upper set) and Pb (lower set), the strongest ice VI peaks again being indicated by asterisks. *Partial* melting is manifested by the appearance of a broad amorphous feature centred near  $2.75 \text{ \AA}$ , the disappearance of most of the ADH IV peaks (residue is marked with arrows), and persistence of the ice VI peaks. Data were not collected at higher temperatures to locate the ice VI liquidus at this pressure.

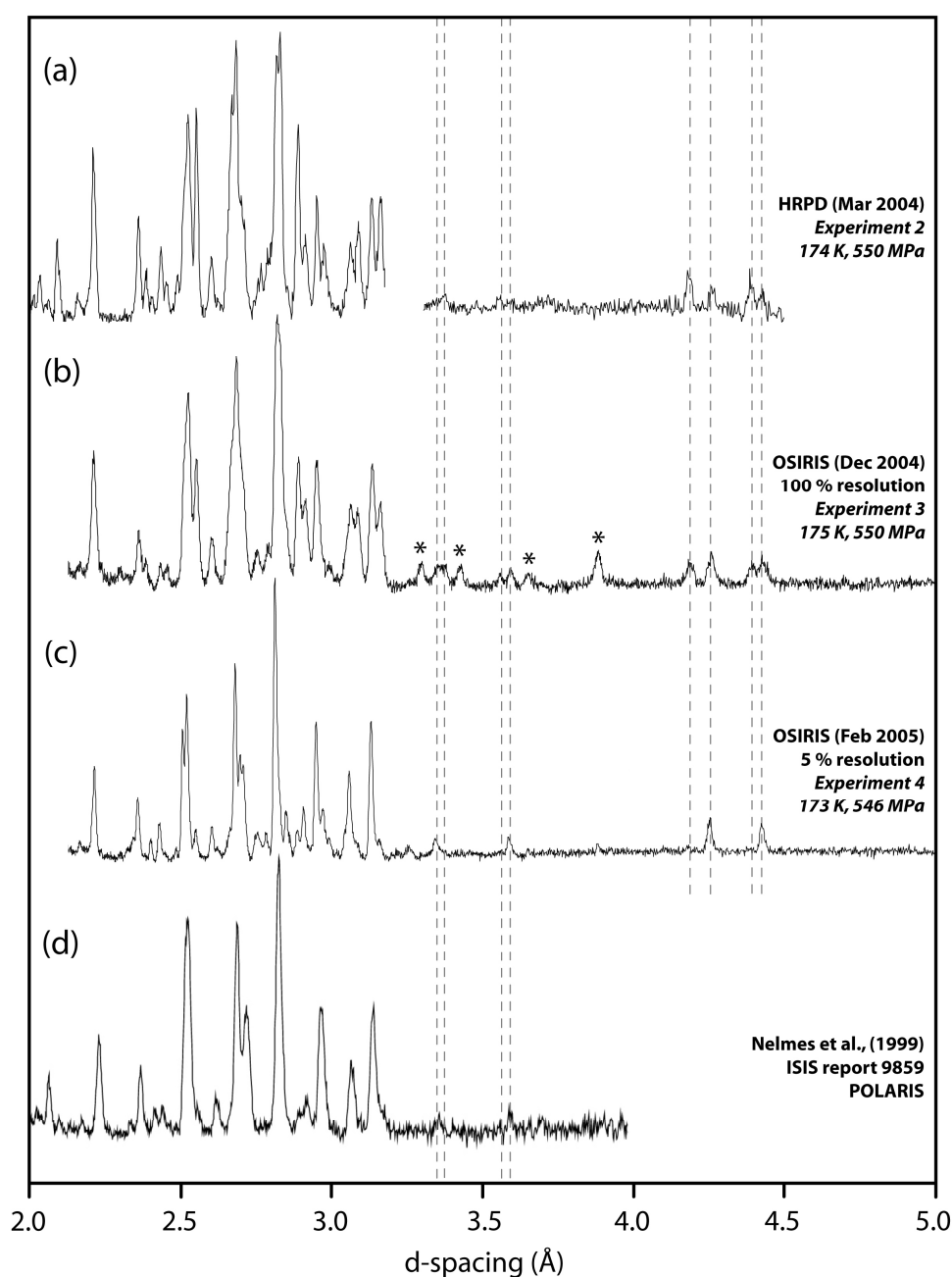


## Electronic supplementary material

### Figure S8: (Experiments 2, 3, and 4)

Comparison of diffraction data collected from ADH II in experiments 2 (pattern a), experiment 3 (pattern b), experiment 4 (pattern c), and by Nelmes *et al.* (1999) (pattern d). Some of the longer d-spacing peaks and their 'satellites' are marked by dashed grey lines. Those peaks marked with asterisks in (b) are unidentified, not being due to AMH I or to any other known phase of ice. As shown in [Figure S3](#), some of the reflections in (c) are due to residual ice IX, ADH I, and AMH I.

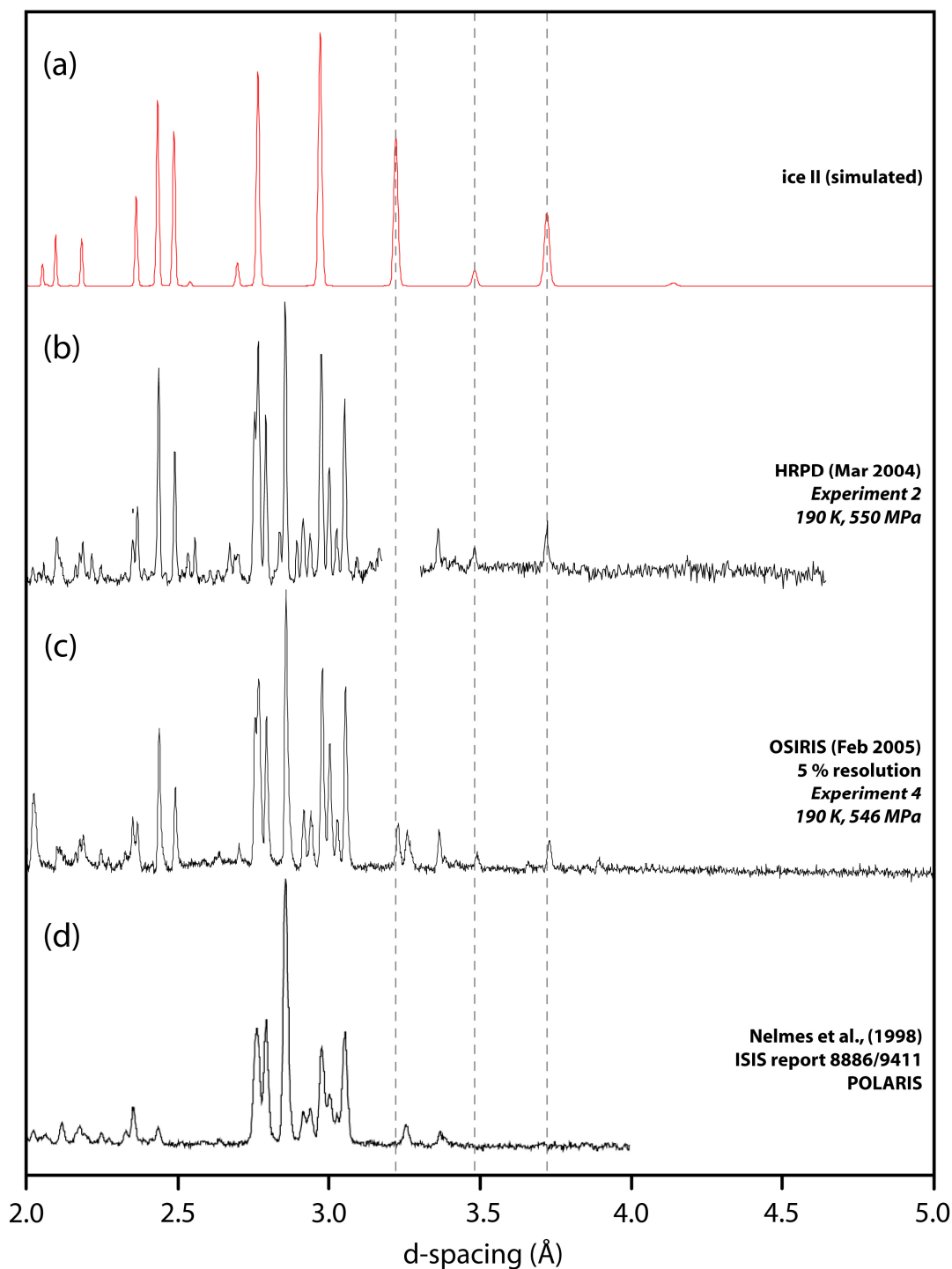
With patterns integrated for a sufficiently long time on OSIRIS, we have the option to use a fraction of the data measured at the largest Bragg angles, affording the highest d-spacing resolution. In [Figures S8c](#) and [S9c](#), we show only the data from the 5 % of detectors at the largest scattering angle; contrast the sharpness of the peaks with those in [Figure S8b](#), which incorporates data from detectors at smaller angles. In the latter instance, the count time was quite short (note the noisier background).



## Electronic supplementary material

### Figure S9: (Experiments 2 and 4)

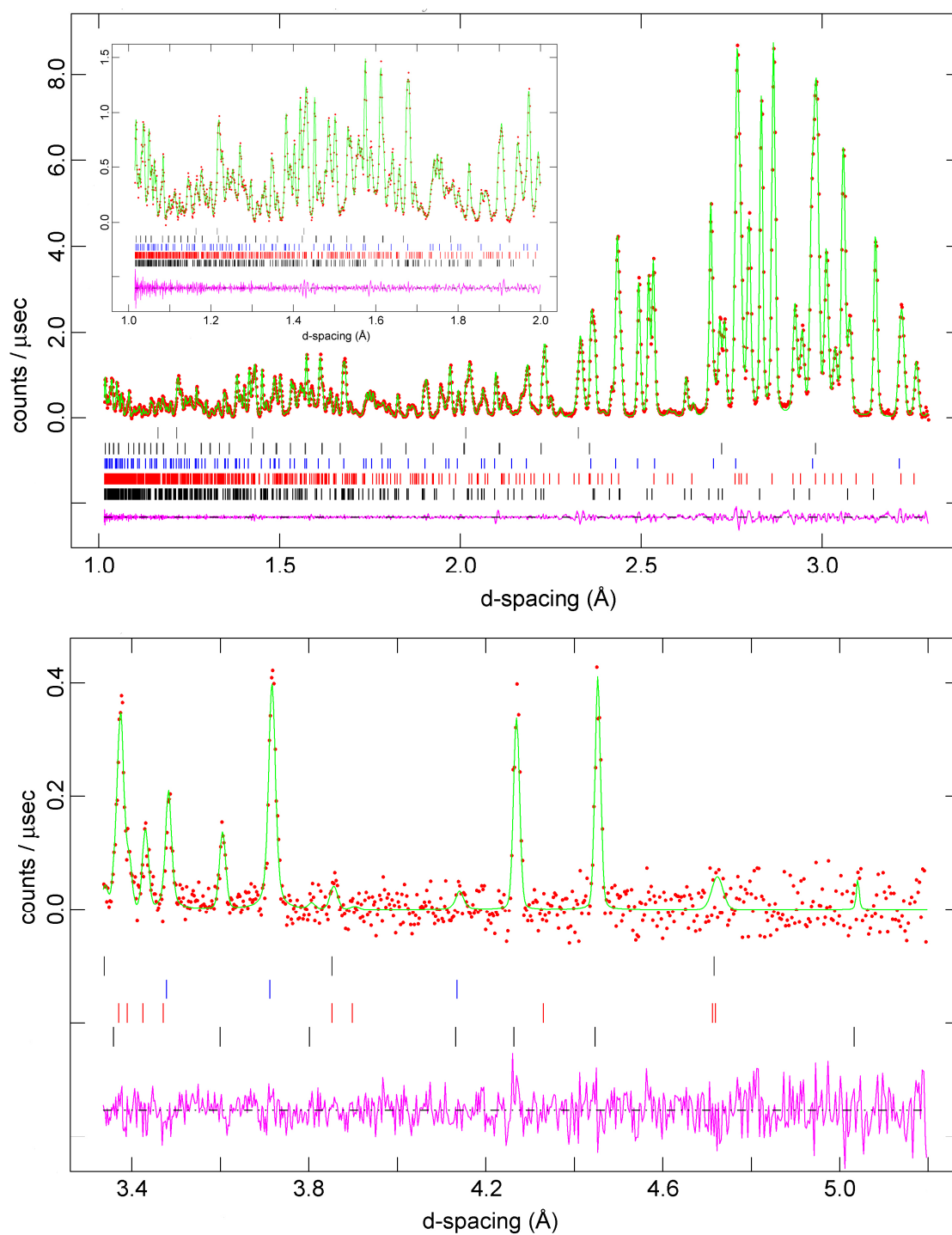
Comparison of diffraction data collected from AMH II during experiment 2 (pattern b) and experiment 4 (pattern c), with the data acquired by Nelmes *et al.* (1998) (pattern d). Outside the strong cluster of AMH II peaks between 2.75—3.05 Å, we observe in particular a strong triplet of peaks between 2.4—2.6 Å, and several smaller reflections in the 3.2—3.7 Å range (highlighted by dashed lines) which are attributable to ice II as shown by the agreement (both in peak position and intensity) with the simulated neutron powder diffraction pattern of ice II (a).



## Electronic supplementary material

### Figure S10: (Experiment 1)

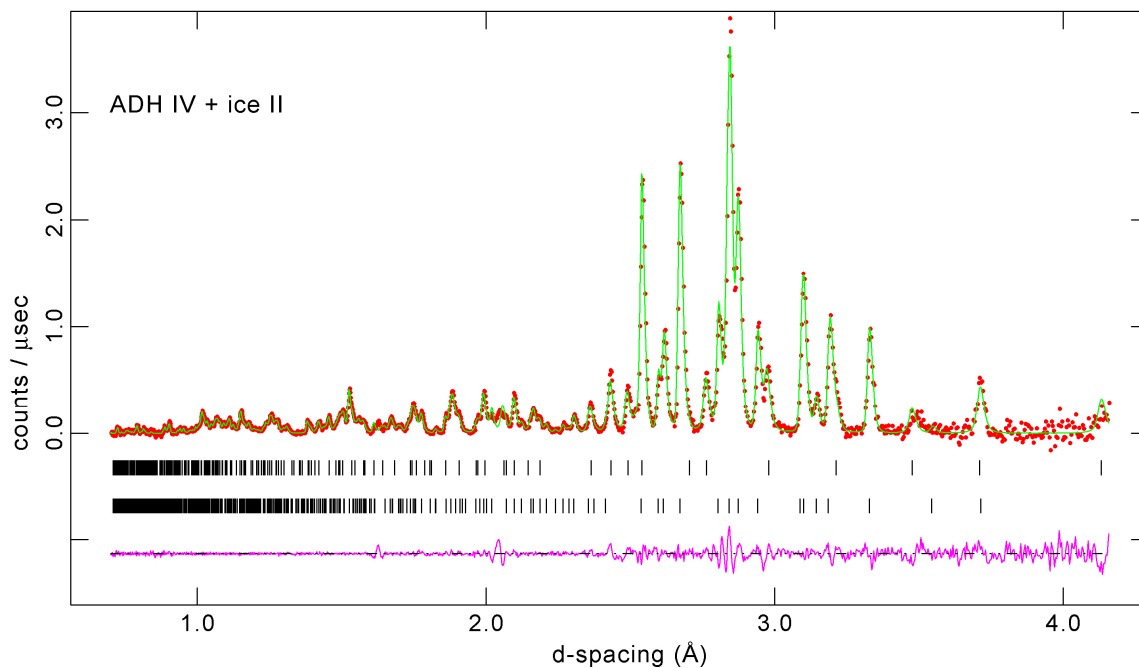
Le Bail profile refinement (green line) of the post-melting diffraction data (red points) collected in experiment 1 at 174 K and 443 MPa. This data contains contributions from several high-pressure polymorphs and from the sample environment; the tick marks represent (from the top down), aluminium, ice IX, ice II, AMH II, and ADH IIa. The powder statistics and unit-cell parameters obtained from this fit are listed in [Table S2](#). The difference between the model and data is indicated by the purple line beneath the tick marks. The inset shows the region from 1—2 Å with an expanded vertical scale.



## Electronic supplementary material

### Figure S11: (Experiment 6)

Le Bail profile refinement (green line) of the 12 hour integration collected at 15.5 tons, 190 K during experiment 6. This data (red points) contains contributions from ice II (upper set of tick marks) and ADH IV (lower set of tick marks). The difference between the model and data is indicated by the purple line beneath the tick marks. The powder statistics and unit-cell parameters obtained from this fit are listed in [Table S3](#).



## Electronic supplementary material

### Supplementary Table 1.

Unit-cell indexings obtained with DICVOL04 for the various crystalline polymorphs observed in our experiments. The figures of merit, M and F, are defined by De Wolff (1968) and Smith & Snyder (1979), respectively.

<b>ADH IIa</b> (monoclinic) (experiment 1, 30—130ms t-o-f window) $a = 7.7876(33) \text{ \AA}$ $b = 6.7269(18) \text{ \AA}$ $c = 6.0746(17) \text{ \AA}$ $\beta = 102.102(27)^\circ$	P = 443 MPa, T = 174 K  V = 311.16 $\text{\AA}^3$ (Z = 4) M(11) = 50.9 F(11) = 55.9 (0.0068, 29)
<b>ADH IIa</b> (monoclinic) (experiment 4) $a = 7.7686(11) \text{ \AA}$ $b = 6.6947(11) \text{ \AA}$ $c = 6.0380(8) \text{ \AA}$ $\beta = 101.967(14)^\circ$	P = 546 MPa, T = 173 K  V = 307.20 $\text{\AA}^3$ (Z = 4) M(11) = 97.1 F(11) = 97.2 (0.0039, 29)
<b>ADH IIb</b> (monoclinic) (experiment 2) $a = 7.8674(19) \text{ \AA}$ $b = 6.7652(11) \text{ \AA}$ $c = 5.9388(10) \text{ \AA}$ $\beta = 102.909(16)^\circ$	P = 550 MPa, T = 175 K  V = 308.10 $\text{\AA}^3$ (Z = 4) M(8) = 130.9 F(8) = 102.5 (0.0029, 27)
<b>AMH II</b> (orthorhombic) (experiment 2) $a = 18.8119(33) \text{ \AA}$ $b = 6.9400(10) \text{ \AA}$ $c = 6.8374(8) \text{ \AA}$	P = 550 MPa, T = 190 K  V = 892.66 $\text{\AA}^3$ (Z = 16) M(12) = 51.5 F(12) = 65.7 (0.0041, 44)
<b>ADH IV</b> (orthorhombic) (experiment 9) $a = 12.5439(68) \text{ \AA}$ $b = 6.6481(24) \text{ \AA}$ $c = 6.3680(25) \text{ \AA}$	P = 740 MPa, T = 190 K  V = 531.05 $\text{\AA}^3$ (Z = 8) M(10) = 27.8 F(10) = 27.0 (0.00112, 33)

## Electronic supplementary material

### Supplementary Table 2.

Powder statistics and refined unit-cell parameters obtained from a Le Bail fit to data acquired after recrystallisation at 443 MPa, 174 K (experiment 1).

		Fitted		Minus background		
Histogram		$N_{\text{data}}$	wRp	Rp	wRp	Rp
90° banks, 30-130 ms t-o-f		1683	1.72 %	1.50 %	1.73 %	1.46 %
90° banks, 100-200 ms t-o-f		635	7.40 %	6.88 %	7.46 %	8.21 %
Total		2318	1.86 %	2.08 %	1.77 %	1.72 %
$\chi^2 = 1.883$						
Phase	$a$ (Å)	$b$ (Å)	$c$ (Å)	$\alpha, \beta, \gamma$	Volume (Å <sup>3</sup> )	
<b>ADH IIa</b>	7.78366(9)	6.72568(7)	6.07443(9)	90°, 102.104(1)°, 90°	310.929(4)	
<b>AMH II</b>	18.86792(20)	6.94772(9)	6.85885(10)	90°, 90°, 90°	899.119(16)	
<b>Ice II<sup>a</sup></b>	12.87078(12)	12.87078(12)	6.18271(10)	90°, 90°, 120°	886.990(16)	
<b>Ice IX</b>	6.6748(3)	6.6748(3)	6.6838(6)	90°, 90°, 90°	297.785(13)	

<sup>a</sup>Triply primitive hexagonal cell ( $Z = 36$ ).

## Electronic supplementary material

### Supplementary Table 3.

Powder statistics and refined unit-cell parameters obtained from a Le Bail fit to data acquired in the P-E cell under a load of 15.5 tons at 190 K (experiment 6). The Rietveld powder statistics are defined in the caption to Table 2.

		Fitted		Minus background		
Histogram		N <sub>data</sub>	wRp	Rp	wRp	Rp
Longitudinal banks		1782	2.38 %	3.42 %	3.35 %	3.32 %
$\chi^2 = 2.378$						
Phase	<i>a</i> (Å)	<i>b</i> (Å)	<i>c</i> (Å)	$\alpha, \beta, \gamma$	Volume (Å <sup>3</sup> )	
<b>ADH IV</b>	12.5626(11)	6.6513(3)	6.3788(3)	90°, 90°, 90°	533.00(4)	
<b>Ice II<sup>a</sup></b>	12.8396(10)	12.8396(10)	6.1628(7)	90°, 90°, 120°	879.86(13)	

<sup>a</sup>Triply primitive hexagonal cell (*Z* = 36).

## Electronic supplementary material

### Supplementary Table 4.

Examples of Avrami constants corresponding to various crystal growth geometries, nucleation rates, and reaction limiting mechanisms.

Geometry	Nucleation, $\alpha$	Interfacial, $n$	Diffusional, $n$
1D	0 (site saturated)	1	0.5
1D	1 (constant rate)	2	1.5
2D	0	2	1
2D	1	3	2
3D	0	3	1.5
3D	1	4	2.5

## Electronic supplementary material

### Supplementary literature citations

- Bauer, M., Elsaesser, M. S., Winkel, K., Mayer, E., & Loerting, T. (2008). *Phys. Rev. B.* **77**, article 220105.
- De Wolff, P. M. (1968). *J. Appl. Cryst.* **1**(2), 108-113.
- Fortes, A. D., Wood, I. G., Alfredsson, M., Vočadlo, L., Knight, K. S., Marshall, W. G., Tucker, M. G., & Fernandez-Alonso, F. (2007b). *High Press. Res.* **27**(2), 201-212.
- Hogenboom, D. L., Kargel, J. S., Consolmagno, G. J., Holden, T. C., Lee, L., & Buyyounouski, M. (1997). *Icarus* **128**(1), 171-180.
- Londono, J. D., Kuhs, W. F., & Finney, J. L. (1993). *J. Chem. Phys.* **98**(6), 4878-4888.
- Loveday, J. S., *et al.* (2009): Observations of ammonia dihydrate in the AMH VI structure at room temperature – possible implications for Titan. Paper submitted to *High Press. Res.*
- Nelmes, R. J., & Loveday, J. S. (1998). Diffraction studies of the low-pressure phases of ammonia hydrates. ISIS Experimental Report RB9411. CCLRC Rutherford Appleton Laboratory ([www.isis.rl.ac.uk/ISIS98/reports/9411.pdf](http://www.isis.rl.ac.uk/ISIS98/reports/9411.pdf)).
- Nelmes, R. J., Loveday, J. S., & Guthrie, M. (1999). Structural changes under pressure in ammonia dihydrate and ammonia hemihydrate. ISIS Experimental Report RB 9859, CCLRC Rutherford Appleton Laboratory ([www.isis.rl.ac.uk/ISIS99/reports/9859.pdf](http://www.isis.rl.ac.uk/ISIS99/reports/9859.pdf)).
- Smith, G. S., & Snyder, R. L. (1979). *J. Appl. Cryst.* **12**(1), 60-65.